WELDABILITY OF AUSTENITIC HEAT-RESISTING STEELS

Elena Grncharevska[1], Elisaveta Doncheva[2], Filip Zdraveski[2], Zoran Bogatinovski[2], Aleksandra Krstevska[2]

[1]PhD Student at the Ss. Cyril and Methodius University in Skopje, Faculty of Mechanical Engineering - Skopje

[2]Ss. Cyril and Methodius University in Skopje, Faculty of Mechanical Engineering - Skopje

Abstract: Austenitic heat-resisting steels are used in a wide range of industries. Their use is motivated not only by their excellent mechanical properties but also due to their excellent resistance to corrosion and the ability to withstand high temperatures. These steels are prone to defects and challenges during welding because of their high content of Cr, Ni, Al, and other alloying elements. The main problem is the high heat energy input, which causes differences in structure between the welded joint and the surrounding area. The relatively high heat input and cooling in the heat-affected zone (HAZ) causes carbide formation and, as a result, coarse grain formation, which is undesirable for obtaining favorable mechanical properties. This study investigates the weldability of two heat-resistant austenitic steels (EN X12CrNi23-13 and EN X8CrNi25-21) using the gas tungsten arc welding (GTAW) technique. Both materials are separately analyzed, and the results are discussed in terms of potential welding techniques and technological plan improvements to achieve high-quality welds without pre-heating or any other additional post-welding heat treatment, which is important for the industry because it can reduce production time and cost.

Keywords: *austenitic heat-resistant steel, coarse grain structure, GTAW, weld metal*

1. Introduction

Greenhouse gas emissions are a major global concern in nowadays living. Thermal power plants contribute to this significantly because fossil fuel combustion is one of the main sources of greenhouse gases [1]. According to research, steam temperature and pressure have a significant impact on a power plant's efficiency [1, 2, 3]. Most of the electricity-generating equipment in power plants operate at very high temperatures from 600°C to 1400 °C and high steam pressures in the range of 20MPa and more [2]. These operating pressures and temperatures are even higher for high-efficiency power plants than they are for conventional older-generation power plants, and as a result, they need less coal to produce the same amount of energy [2, 4]. As operating temperatures rise, structural components must meet higher standards for use in power plants with high temperatures. As a result, a variety of heat-resistant steels have been created [1] that can withstand harsher operating conditions to meet these demands. While the operating conditions don't call for any special mechanical characteristics, they do call for strong anti-corrosion and high resistance to heat destruction. Low-alloy steels cannot be used in hostile environments or at temperatures higher than 550°C because they lose strength at high temperatures and form a thick layer of oxide. To avoid additional costs, steel microstructure must remain stable over an extended period while operating defect-free. When conventional steel is exposed to high temperatures, strengthening precipitates dissolve or coagulate, which significantly reduces strength and mechanical properties and speeds up corrosion [4]. These unfavorable conditions could result in failures.

Heat-resistant steels themselves belong to the group of high alloy steels and the basic alloying element added to steel is Cr. With a greater presence of chromium (Cr), the heat resistance increases, and with the presence of other alloying elements such as Ni, Al, Mo, Ti, etc. the steel improves the mechanical properties. Based on the microstructural characteristics these steels can be ferritic steels with main alloying elements (Cr, Si, and Al), ferritic-austenitic steels, ferritic-martensitic steels, martensitic and austenitic steels with main alloying elements (Cr, Ni, Si, and less frequently Al and Ti).

Two types of heat-resistant steels are used in power plants: ferritic-martensitic and austenitic steels [2]. The ferritic-martensitic grades include trace amounts of Mg, Mo, S, C, and Ni, which are primarily present to aid in precipitation strengthening and high-temperature behavior [2]. The martensitic steels are designed for operation at steam temperatures below 650 °C [2,5]. The main steam pipes in fossil power plants with steam temperatures up to 600 °C have frequently been made of martensitic heat-resistant P91 and P92 steels [1]. In comparison to martensitic heat-resistant steel, austenitic heat-resistant steel has a higher resistance capability to oxidation [1]. Also, austenitic steels are significantly stronger, more ductile, and have a higher creep-rupture strength than ferritic/martensitic steels [2]. These steels are widely used in many industries like chemical, pharmaceutical, cement, and food industries, as well as in aviation, navy, and architecture. This is due to their superior cold hardening and polishing capabilities, high oxidation and corrosion resistance,

mature manufacturing process, good deformation, and mechanical properties at elevated temperatures [5, 6]. However, due to the formation of carbides and nitrides in the microstructure, which coarsens during use, commercial heat-resistant austenitic steels have low creep rupture strengths at high temperatures [7, 8]. The carbides at the boundaries are the ideal location for cavity nucleation under creep-fatigue loading conditions, which calls into question the creep-fatigue life of the structure.

Austenitic stainless steels are also used when joining dissimilar metals [9]. The tensile strength of joints between structural C-steel and austenite stainless steel was studied by Cam et al. in a recent publication [9]. They discovered that joints fracture at low-strength base metal sides and that there are certain inhomogeneities in the weld metal microstructure, which contained three phases: ferritic-austenitic, baintic, and martensitic phases. Welding can be difficult because residual stresses in the joint may result from the different thermal conductivities of austenitic stainless steel and carbon steel [9]. As opposed to welding martensitic and ferritic steels, welding austenitic heat-resistant steels only presents two difficulties: poor heat dissipation and increased electrical resistance. Intergranular corrosion can happen in the base material as well as the heat-affected zone (HAZ). It's also possible that internal stresses contribute to the formation of hot cracks during the weld cooling process. Austenitic heat-resistant steels contain different amounts of alloying elements which can allow steel to pass through the precipitates during service and thus provide high-temperature stress strength, grain refinement, and precipitation hardening [10]. But when the welding process is used these characteristics might change, because of the effect of the localized high temperature [10], so it is important to study the creep rupture strength and mechanical properties of welded joints of these steels.

In the present research, the weldability of two types of austenitic heat-resistant steels (X12CrNi23-13 and X8CrNi25-21) is investigated. The experiment consists of welding two samples from both materials with gas tungsten arc welding (GTAW) with assigned parameters according to the assigned welding technology. After welding the samples, several tests were done bending, hardness, tension, non-destructive tests with penetrants, and radiography. The findings demonstrate that it is possible to reduce the cost of welding during the construction of structures by adjusting some of the parameters, such as current strength and welding speed. By doing so, it is possible to avoid preheating and additional heat treatment during the welding of these pieces. Additionally, data on critical properties and information on the microstructural characteristics are provided. The study's main objective is to offer an initial understanding of the mechanical and weldability characteristics of austenitic heat-resistant steels. It identifies potential next steps for additional research, and the findings can act as a fundamental manual for welding these steels with GTAW.

2. Materials, experiments, and methods

The two welded plates used in the investigation are made of two different austenitic heat-resistant steel plates with the designations EN X12CrNi23-13 and EN X8CrNi25-21. The mechanical characteristics and chemical composition of these steels are listed in Tables 2.1 and 2.2.

Table 2.1 *Mechanical properties of austenitic heat-resistant steels*

Designation		Mechanical properties					
EN	AISI	R_m	$R_{p0,2}$	A_5	Z	KU	HB
		N / mm²		%	%	J	
X12CrNi 23-13	S309	500-700	210	35	43	21	192
X8CrNi2 5-21	S310	500-700	210	35	42	23	192

Table 2.2 *Chemical composition of austenitic heat-resistant steels*

Designation		Chemical composition %							
EN	AISI	C	Si	Mn	P	S	Cr	Ni	N
X12CrNi23-13	S309	0.15	1	2.0	0.045	0.015	22.0-24.0	12-14	0.11
X8CrNi25-21	S310	0.10	1.5	2.0	0.045	0.015	24.0-26.0	19.0-22.0	0.11

Data from both tables indicate that there are only minor variations in the Cr and Ni contents between these materials. The dimensions of the plates are 150 x 150 x 2.5mm and 150 x 150 x 6mm. The welding technique used is GTAW with different welding parameters for each set of plates. The welding on the

thinner plate (sample 1) is a two-sided facing joint with one passage. The thicker plate (sample 2) is prepared with X shaped grove for a butt-weld joint done with several passes, performed using the same device (Cea Matrix 250 HF) that was used for welding the thinner plate. The temperature of the workpieces before welding and between each pass is measured with an infrared thermometer Steinel HL Scan. The protective gas during the welding of both materials is Argon with a content of 99.99% due to the provision of deeper penetration and quality protection of HAZ from inclusions from the atmosphere. The flow is 14 l/min. The filler material for both steels is an EZ – TIG 309L Si2.4 bar with a diameter of 2.0mm. At a 23°C ambient temperature, sample 1 is welded without any preheating. A 64A current is used for the frontal pass, which is followed by a 29°C cooling period before the next pass is made on the opposite side. The sample is rotated, cleaned at the root, and then welded using the same 64A current. Following the application of the first layer, the piece is rotated once more to the opposite side for the application of the second pass, which uses a current of 62A. Since the time between these operations is short, the intermediate temperature remains at the value of 50°C. After the second side of the joint has been welded, the object is removed from the worktable, visually inspected, and then cooled in air. Figure 2.1 illustrates the pre-welding preparation, the welding process, and the deformation that results from too much heat being applied to the material. The short cooling period the piece had between rotation and the other side's welding is what caused the deformation.

Figure 2.1 *Pre-welding preparation, welding, and deformation after welding of Sample 1*

The second sample is also welded without preheating at an ambient temperature of 23°C and the preparation of the sample is shown in Figure 2.2. The second sample is welded on two sides, with three passes on each side with the same device as the first sample with argon as a protective gas. The filler material used has a diameter of 2mm, and the tungsten electrode used has a diameter of 2.4mm. The values for the current and the various temperatures between the layers are shown in Table 2.3.

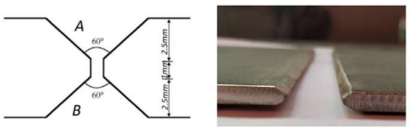

Figure 2.2 *Sample 2 preparation with X-shaped grove for butt welded joint.*

Table 2.3 *Current used and temperature measured between layers*

Pass number	Current used [A]	Temperature measured in between layers [°C]
1	93	20
2	93	152
3	109	47
4	109	100
5	120	52
6	120	159

The filler material for both steels is an EZ – TIG 309L Si2.4 bar with a diameter of 2.0mm and mechanical properties and chemical composition shown in Table 2.4 and Table 2.5.

Table 2.4 Mechanical properties of filler material

Designation	Mechanical properties			
W 23 12 L Si	R_m [N/mm²]	$R_{p0.2}$ [N/mm²]	A5	Z
	510	320	-	-

Table 2.5 Chemical composition of filler material

Designation	Chemical composition %					
W 23 12 L Si	C	Si	Mn	P	Cr	Ni
	0.03	0.76	1.32-	0.0022-	23.65	12.76

To prove the quality of the welded joints, several tests are done that can be categorized as non-destructive (penetrants and radiography) and destructive testing (macrostructure and microstructure examination, hardness testing, bending and tensile testing). The radiographic method includes an examination for detecting errors in the welded joint: cracks, slag inclusions, porosity, and unpenetrated root. The samples were tested according to the standard EN 17636-1. The source is 2x2 in size and emits X-rays. The irradiation time is 30s for sample 1 and 42s for sample 6mm. According to the EN 3452 standard, penetrant testing entails the following steps: cleaning and degreasing the surface of the material being tested, application of the penetrant, removal of the penetrant with water or a cloth, and application of a developer that draws the penetrant out of the cracks. These procedures were carried out on both samples. Two

testing samples are created from both welded plates for the macrostructure examination, as shown in Figure 2.3.

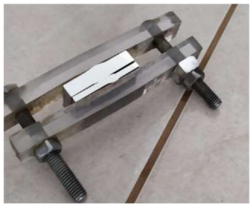

Figure 2.3 *Testing samples for observation of macrostructure on both welded plates*

Additionally, tests for hardness, bending, and tensile strength have been conducted. Figure 2.4 displays the samples from these tests for both materials.

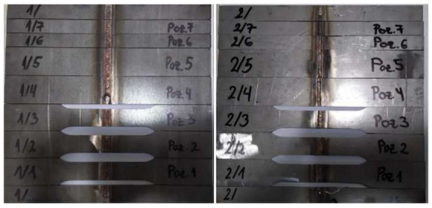

Figure 2.4 *Testing samples for tensile, bending and hardness testing*

The label's first number denotes the sample's number, and its second number, the location of the testing sample.

The hardness testing is carried out according to standard EN 6507-1 with a diamond indenter tool with hardness 10HV. Although the indented samples can be ground and polished for microstructure analysis, other samples were created for this study's microstructure analysis. These were ground and polished in preparation for microstructure analysis. The polishing step was done with a polisher cloth and the addition of Al_2O_3 with gradation up to 5µm. The samples were quickly dried after being etched for a brief period with a V 2A etchant. Later, the structure is examined under an optical microscope, and pictures are created for later analysis. Using bend testing of the butt-welded joints in accordance with standard EN 910, the capacity of the austenitic heat-resistant steels to bend around the welded joint was investigated. A pin with a 4a diameter is used to bend the samples around the welded joint face and welded joint root at an angle of up to 120 degrees. The pin is 15mm wide and passes between the cylinders. Figure 2.5 shows the procedure for both samples. For the bend test result to be considered acceptable, neither the weld nor the metal should have failed.

The standard tensile testing machine SHIMADZU, which has a maximum capacity of 250kN, is used for the tensile testing. Three specimens from each welded plate with dimensions in accordance with ISO6892 and EN895-Part 1 are tested on a total of six samples. The test is conducted at a 5 mm/min speed.

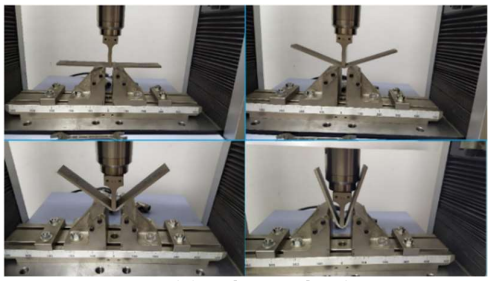

Figure 2.5 *Tripple point bending testing.*

The tensile tests were performed with an accuracy of 0.001 mm at room temperature. The samples prepared for this testing are shown in Figure 2.6.

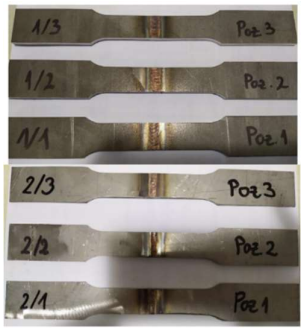

Figure 2.6 *Tensile testing specimens*

3. Results and discussions

In sample 1, unpenetrated roots and many pores with dimensions that do not meet the requirements for a high-quality welded joint were observed. Only a few minor pores were found in the second sample, which are not thought to be important for the joint's capacity to support weight. Due to the careful selection of the X-grove plate preparation, the multiple passes of welding, and the maintained temperature between them, the second sample has a higher quality. Figure 3.1 displays both radiograms. The results from penetrant testing demonstrated that the weld and its surrounding area are free of any defects.

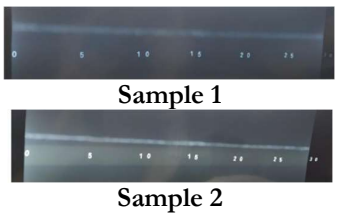

Sample 1

Sample 2

Figure 3.1 *Sample 2 preparation with X-shaped grove for butt welded joint.*

The metallographic examination (macroscopic and microscopic examinations) is carried out to ascertain

the fundamental structure of the austenitic steel and to determine the quality of the produced welded joint in terms of defined eligibility criteria according to standard EN288-3. The macrostructure of the welded samples is shown in Figure 3.2.

Figure 3.2 *Macrostructure of welded joints in both samples*

The base metal, the heat-affected metal, and the weld metal, which expresses the groove fill area, are shown as the components of the welded joint in Figure 3.2. The macrostructures of the welded joint samples under examination demonstrate that the welding process and selected welding technology have been met in full. In Figure 3.3 the micrographs demonstrate the microstructures of 3 specific zones: base metal, HAZ and weld metal for sample 1 on the left side and sample 2 on the right side.

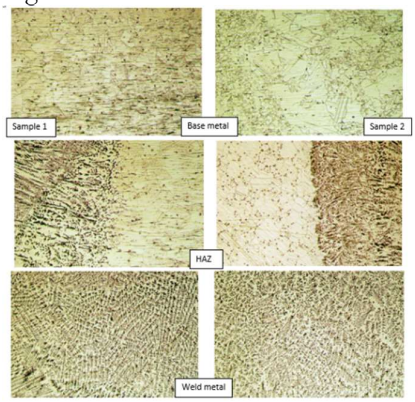

Figure 3.3 *Microstructure in base metal, weld metal and HAZ for Sample 1 (left side) and Sample 2 (right side)*

The base metal for both samples shows a typical austenitic grain matrix containing annealing twins and some non-metallic inclusion. The micrographs that represent the heat-affected zone on both samples, clearly indicate the changes from the composition of the base metal to weld metal. The transition zone is dendritic with a coarser grain structure and a new phase that is emerging within the grains, a dense and dark microconstituent that resembles a perlite structure. There is a presence of precipitated carbides inside and along the grain boundaries, as well as a slight rounding of the grains, which are both caused by the heat input. Sample 2 is characterized by cellular dendritic microstructure, and in Sample 1 the overlay is a bit different the cells and dendrites are not always well-defined. It is generally accepted that the ratio of chromium equivalent (Creq) to nickel equivalent (Nieq) determines the solidification microstructure [11]. There are several causes for the formation of these differences in the microstructures. Different microstructures that form in both grades of stainless steel may be explained by differences between the solidification modes of these materials (sample 1- 309S and sample 2 – 310S). The primary phase formed during the 310S solidification is austenite and when cooled to room temperature, this austenite doesn't change. Weld metal has a distinctive dendritic structure with large, elongated grains, and it seems that the grain size and the twins of the specimens experienced significant changes during the thermal cycles caused by the welding. The grains are larger and elongated, the twins are thicker. The images make it obvious that the most crucial component of the welded joint is the transition between the Heat Affected Zones and weld metal. There are noticeable differences in the size and shape of the formed grains, which makes that area more brittle. Therefore, for more in-depth analysis, a 500:1 magnification is required.

There are no extreme differences in hardness between the base metal, HAZ, and weld zone. There is a slight rise in hardness in the second sample in the weld zone which is expected. On the contrary, the first step shows an undermatch case of weld the hardness in the base metal is higher than the one measured in the welded zone. Due to the limitations of optical measurement and the imperfections in the tip geometry, the results are characterized by significant uncertainties. The differences between these zones can be more accurately measured if a smaller indentation tool is used. Results from hardness testing are given in Figure 3.4.

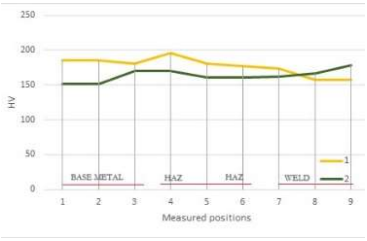

Figure 3.4 *Hardnes testing results for samples 1 and 2*

The bending test results for specimens from both welded plates indicate that the performed welding process is of high quality since there were no signs of cracks upon reaching the bend angle of 120^0. No discernible difference was found between the specimens based on the measured angles. Due to the material's high strength and the lack of a machine that

can handle the demands of this kind of material, the samples failed to break. However, the value is greater than the necessary service value, leading to the conclusion that the weld satisfies the requirements for bending. In the first sample, the fracture occurs in the base material, while in the second sample, the fracture precisely occurs in the zone that separates the base metal from the weld metal, as shown in Figure 3.5.

Figure 3.5 *Bending testing samples*

All measured angles and the maximum load in samples taken from the sample 1 and sample 2 welded plates are listed in Table 3.1.

Table 3.1 *Angles and maximal loading during the bending test*

Sample	1.1	1.2	2.1	2.2
α [⁰]	136	136	140	122
F [N]	6056.72	6027.22	6981.09	6656.28

Tensile testing results revealed consistency in measurements, and measured sizes were roughly the same in each test specimen that was observed. According to Figures 3.6 and 3.7, the fracture for the specimens from the thinner plate occurs in the base metal as opposed to the specimens from the second plate, where the fracture occurs precisely in the heat-affected zone, which is the zone between the base metal and the weld.

Figure 3.6 *Tensile test specimens from sample 1*

Figure 3.7 *Tensile test specimens from sample 2*

Figure 3.8 displays the test results for each of the six specimens. Thicker plate samples exhibit higher yielding and maximum stress than thinner plate samples. Only one sample from the thicker plate fractured in the welded zone; the welds in the thinner plate samples did not fail.

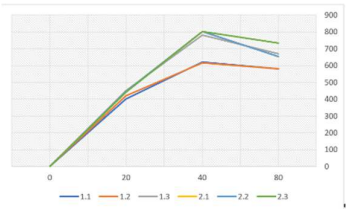

Figure 3.8 *σ – ε diagram for each tensile test specimen*

4. Conclusions

The impact of the welding process, or the choice of the welding process technology, on mechanical and operational properties, is carefully examined based on several variables that accurately describe the behavior of the base metal, welded joint, and its component parts. Chemical microsegregation during solidification facilitates the understanding of microstructure formation in austenitic steel weld overlays. Each weld overlay has a microstructure that is typical of the cast microstructure of a complex alloy, where the chemically homogeneous liquid phase solidifies into a less homogeneous solid. Along with evaluating the quality of the welding technology that has been used, this examination also establishes the boundaries of the various structures that comprise the welded joint. Further research on austenitic heat-resistant steels can be done using the properties that were examined in this study. Since the thicker sample that was welded produced better results, it can be used to conduct additional research on how high temperatures affect mechanical properties while still utilizing the same welding technique.

References

[1] L. Xu, S. Yang, L. Zhao, Y. Han, H. Jing, and K. Wang, “Low cycle fatigue behavior and microstructure evolution of a novel Fe-22Cr-15Ni austenitic heat-resistant steel,” *Journal of Materials Research and Technology*, vol. 9, no. 6, pp. 14388–14400, Nov. 2020, doi: https://doi.org/10.1016/j.jmrt.2020.09.121.

[2] Z.-F. Hu, “Heat-Resistant Steels, Microstructure Evolution and Life Assessment in Power Plants”, Thermal Power Plants. InTech, Jan. 13, 2012. doi: 10.5772/26766.

[3] Y. Zhou *et al.*, “Precipitation behavior of type 347H heat-resistant austenitic steel during long-term high-temperature aging”, *Journal of Materials Research*, vol. 30, no. 23, pp. 3642–3652, Nov. 2015, doi: https://doi.org/10.1557/jmr.2015.343.

[4] B. Rutkowski, “Microstructural Characterisation of Austenitic Heat Resistant Sanicro 25 Steel after Steam Oxidation”, *Materials*, vol. 13, no. 15, p. 3382, Jul. 2020, doi: https://doi.org/10.3390/ma13153382.

[5] Y. Xu *et al.*, “Microstructure and Mechanical Properties of an Austenitic Heat-Resistant Steel after Service at 570 °C and 25.4 MPa for 18 Years”, *Journal of Materials Engineering and Performance*, vol. 30, no. 2, pp. 1030–1038, Jan. 2021, doi: https://doi.org/10.1007/s11665-020-05420-6.
[6] M. Sroka, A. Zieliński, G. Golański, Mirosława Pawlyta, H. Purzyńska, and František Nový, “Evolution of the microstructure and mechanical properties of Sanicro 25 austenitic stainless steel after long-term aging”, *Archives of Civil and Mechanical Engineering*, vol. 23, no. 3, May 2023, doi: https://doi.org/10.1007/s43452-023-00690-y.
[7] H. Ishikawa, C. Zhang, S. Chen, and Z. Yang, “Precipitate Behavior in Fe–20Cr–30Ni–2Nb Austenitic Heat-Resistant Steel”, *Acta Metallurgica Sinica (English Letters)*, vol. 28, no. 4, pp. 424–429, Jan. 2015, doi: https://doi.org/10.1007/s40195-015-0212-1.
[8] L. Wei *et al.*, “Prediction of High-Temperature Creep Life of Austenitic Heat-Resistant Steels Based on Data Fusion”, *Metals*, vol. 13, no. 9, p. 1630, Sep. 2023, doi: 10.3390/met13091630
[9] M. Hietala, M. Jaskari, M. Ali, A. Järvenpää, and A. Hamada, “Dissimilar Laser Welding of Austenitic Stainless Steel and Abrasion-Resistant Steel: Microstructural Evolution and Mechanical Properties Enhanced by Post-Weld Heat Treatment,” *Materials*, vol. 14, no. 19, p. 5580, Sep. 2021, doi: https://doi.org/10.3390/ma14195580.
[10] Li, Xinmei et al. “Stress Rupture Properties of Welded Joints of Austenitic Heat-resistant Super304H Steel at 650 °C”, *IOP Conference Series: Materials Science and Engineering* 711 (2020): n. pag.
[11]M. Rozmus-Górnikowska, S. Dymek, M. Blicharski, Ł. Cieniek, and J. Kusiński, “Microstructure of 309 and 310 Austenitic Stainless Steel CMT Overlays on the 16Mo3 Pressure Vessel Steel,” *Archives of Metallurgy and Materials*, vol. vol. 66, no. No 2, pp. 645–649, May 2021, doi: https://doi.org/10.24425/amm.2021.135902.]